ACS APPLIED MATERIALS & INTERFACES

Research Article

www.acsami.org

Synthesis of Ultrathin Poly(methyl methacrylate) Model Coatings Bound via Organosilanes to Zinc and Investigation of Their Delamination Kinetics

Danish Iqbal, Julian Rechmann, Adnan Sarfraz, Abdulrahman Altin, Georgi Genchev, and Andreas Erbe*

Max-Planck-Institut für Eisenforschung GmbH, Department of Interface Chemistry and Surface Engineering, Max-Planck-Str. 1, 40237 Düsseldorf, Germany

ABSTRACT: Polymer coatings are widely used to protect metals from corrosion. Coating adhesion to the base material is critical for good protection, but coatings may fail because of cathodic delamination. Most of the experimental studies on cathodic delamination use polymers to study the corrosion behavior under conditions where the interfacial chemistry at the metal(oxide)/polymer interface is not well-defined. Here, ultrathin linear and cross-linked poly(methyl methacrylate) [PMMA] coatings that are covalently bound to oxide-covered zinc via a silane linker have been prepared. For preparation, zinc was functionalized with vinyltrimethoxysilane (VTS), yielding a vinyl monomer-covered surface. These samples were subjected to thermally initiated free radical polymerization in the presence of methyl methacrylate (MMA) to yield surface-bound ultrathin PMMA films of 10−20 nm thickness, bound to the surface via Zn−O−Si bonds. A similar preparation was also carried out in the presence of different amounts of the cross-linkers ethylene glycol diacrylate and hexanediol diacrylate. Functionalized and polymer-coated zinc samples were characterized by infrared (IR) spectroscopy, secondary ion mass spectrometry (SIMS), ellipsometry, and X-ray photoelectron spectroscopy (XPS). Coating stability toward cathodic delamination has been evaluated by scanning Kelvin probe (SKP) experiments. In all cases, the covalently linked coatings show lower delamination rates of 0.02−0.2 mm h^{-1} than coatings attached to the surface without covalent bonds (rates ∼10 mm h^{-1}). Samples with a higher fraction of cross-linker delaminate slower, with rates down to 0.03−0.04 mm h^{-1}, compared to ∼0.3 mm h^{-1} without cross-linker. Samples with longer hydrophobic alkyl chains also delaminate slower, with the lowest observed delamination rate of 0.028 mm h^{-1} using hexanediol diacrylate. For the coatings studied here, delamination kinetics is not diffusion limited, but the rate is controlled by a chemical reaction. Several possibilities for the nature of this reaction are discussed; radical side reactions of the oxygen reduction are the most likely path of deadhesion.

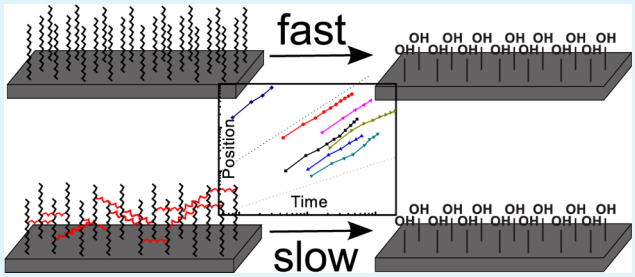

KEYWORDS: *cathodic delamination, corrosion protection, zinc, organic coatings, polymer brushes, grafting*

1. INTRODUCTION

Corrosion of metals causes annual losses of several % of the world gross domestic product.[1] To enhance the corrosion resistance of galvanized steel or ungalvanized steel, these are often coated with polymers.[2−4] However, achieving durable adhesion at the metal(oxide)/polymer[5] interface is always a challenge: deadhesion of polymer coatings from the metal or oxide substrate due to corrosive electrochemical processes is a common problem which could lead to complete loss of desired material properties. Regarding steel, including galvanized steel, as well as zinc, cathodic delamination starting on an electrolyte-filled defect is one of the main mechanisms of coating deadhesion.[2,3,6]

The electrochemistry of cathodic delamination has been widely investigated by scanning Kelvin probe experiments, which lead to a detailed understanding of the electrochemical aspects of the deadhesion mechanism.[7−12] In cathodic delamination, a galvanic cell is formed, where oxygen reduces at a local cathode which propagates under the coating, while metal dissolves at the local anode in the region where delamination has already occurred. Oxygen reduction results in the formation of hydroxide ions, which cause a pH rise near the delamination front. Subsequently, deadhesion of polymer coating from the metal(oxide)/polymer interface is observed.[11] However, the nature of the bond which is actually broken during the deadhesion process is not easy to assess.

A more general problem in polymer adhesion, which is particularly striking in the study of delamination processes, is the lack of detailed knowledge about the chemistry at the polmer/metal or polymer/oxide interface.[13,14] The direct analytic probing of such a buried interface is difficult, as most available nondestructive experimental techniques are not interface specific, with the notable exception of sum-frequency generation spectroscopy.[15,16] Therefore, typically, the interface is destroyed, and subsequently, the detailed analytical features of surface analysis are available.[9,17,18] As a pure analytic

Received: July 28, 2014
Accepted: September 18, 2014
Published: September 18, 2014

approach to an understanding of metal(oxide)/polymer interfaces can give only limited answers, here we use a synthetic approach, in which the metal(oxide)/polymer interface is defined by chemical synthesis.

Polymer adhesion to oxide-covered metals can be significantly enhanced when van der Waals interactions are replaced by covalent bonding.[18,19] Covalent bonding leads to an enhanced resistance of polymer coating against cathodic delamination. Covalently bound polymer coatings on inorganic substrates are typically synthesized by two routes (a) a grafting to approach,[20−24] where presynthesized end functionalized polymers are covalently bonded to the substrate or (b) a grafting from/onto approach,[24−29] where polymer is grown in situ on the solid substrate. A special case is an ultrathin, highly cross-linked plasma polymer film.[30−33]

Cathodic delamination studies have recently focused on the role of ion transport,[17,34,35] including quantification of transport rates.[36] Migration, rather than diffusion, has been shown to be an important process for transport along the interface.[37] The effect of surface morphology was also investigated.[38,39] Comprehensive parameter scans have been carried out.[40] For a better understanding of the chemical processes, delamination experiments have been combined with infrared spectroscopy.[41] Mathematical models of the electrochemical processes have been developed, which permit a detailed analysis of the kinetics.[42] Most studies leave the surface chemistry ill-defined or use complex industrial coatings, which permit only a global understanding of the processes. Nevertheless, the detailed understanding of the electrochemistry has led to novel coatings with self-healing properties.[43,44]

Investigations of the direct linkage of coatings to the surface is a subject of current interest[18] and, e.g., bifunctional silane linkers have been found to decrease degradation rates.[19] To overcome problems with the definition of interfacial chemical bonds, we present here an approach were an ultrathin polymer coating was synthesized. Metallic zinc substrates were modified with vinyltrimethoxysilane (VTS), defining the covalent linkage at the metal(oxide)/polymer interface. Subsequently, these surface-functionalized zinc substrates were subjected to a thermally initiated copolymerization of methyl methacrylate (MMA) in the presence or absence of cross-linkers. Resulting poly(methyl methacrylate) [PMMA] coatings have been characterized, and their delamination behavior has been studied using scanning Kelvin probe (SKP) and electrochemical linear polarization experiments.

2. EXPERIMENTAL SECTION

2.1. Materials. Zinc sheets (purity, 99.95%) with a thickness of 1.5 mm were obtained from Goodfellow (Cambridge, UK). VTS, ethylene glycole diacrylate (EDA), hexanediol diacrylate (HDA), MMA, azobis(isobutyronitrile) (AIBN), toluene, and ethanol were supplied by Sigma-Aldrich (Steinheim, Germany). MMA was purified by distillation from CaH_2 under a N_2 atmosphere, while AIBN was recrystallized in ethanol prior to use.[45] All other chemicals were used as received unless otherwise noted. Zinc substrates (15 mm × 15 mm) were initially mechanically ground with SiC paper up to 4000 grit, followed by polishing with silicon paste (1 μm) to have a smooth surface. Polished samples were ultrasonically cleaned in acetone and dried under a nitrogen stream. Prior to functionalization, zinc substrates were immersed in 0.1 M NaOH for 1 min to increase the concentration of hydroxyl groups.[11] The substrates were then thoroughly washed with deionized water. All synthesis steps were performed under air exclusion in standard Schlenk tubes.

2.2. Surface Modification. The overall surface modification is illustrated in Scheme 1. After the hydroxide treatment, zinc surfaces were modified with VTS by a silanization reaction,[46] to obtain a vinyl-terminated, silane modified substrate. Functionalization was carried out at room temperature by immersion of a polished zinc substrate in an ethanol/water mixture (90:10) containing 0.007 M of VTS. After 24 h, the sample was removed, cleaned sequentially with excess acetone and ethanol to remove physisorbed molecules, and dried under a pressurized nitrogen stream.

Scheme 1. Scheme of the Surface Modification Steps Carried out in This Work

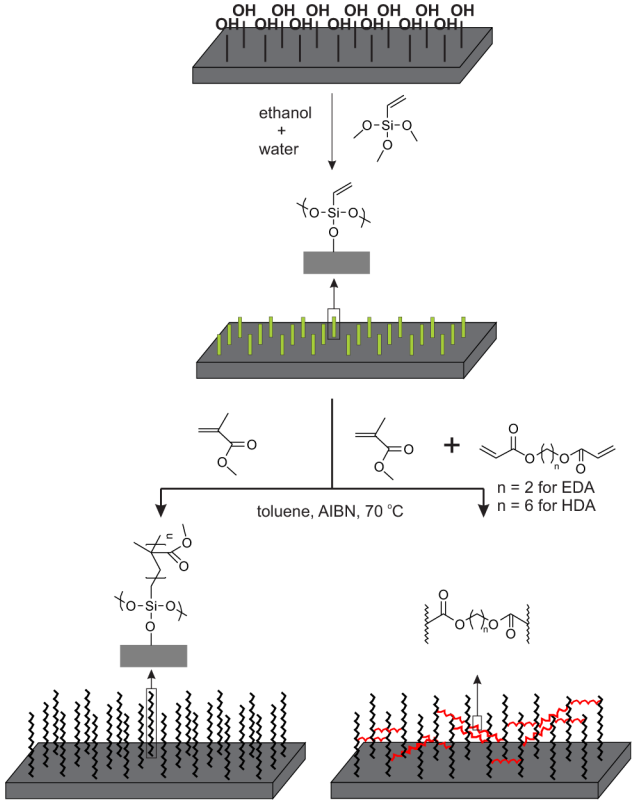

For polymerization reactions, initially, toluene (40 mL) was degassed by performing three freeze−thaw−pump cycles. Subsequently, MMA was added to reach a final concentration of 0.007 M, and AIBN was added to the solution in a concentration of 1 wt % relative to MMA. The mixture was stirred until a homogeneous solution was obtained. A functionalized zinc sample was then introduced into the reaction mixture, and the temperature was raised to 70 °C in order to initiate a polymerization reaction. After 24 h, the zinc sample was removed and washed with excess acetone, followed by ultrasonic cleaning for 1 min in a toluene solution in order to remove any remaining traces of polymer which is not covalently linked to the zinc. Later, the samples were dried in a nitrogen stream.

For the preparation of polymer coatings with different cross-linking densities on zinc substrate, the same polymerization procedure was employed, with different molar fractions (25% or 50%) of the respective cross-linking agent (EDA or HDA) added to the solution. The total monomer concentration (EDA/HDA + MMA) was kept constant.

2.3. Characterization Methods. Modified samples were characterized by infrared (IR) spectroscopy on a Bruker Vertex 70v Fourier transform IR spectrometer (Bruker, Karlsruhe, Germany). Reflectance IR spectra of functionalized and polymer-coated zinc samples were taken with a spectral resolution of 4 cm^{-1} at an angle of incidence of 80° using p-polarized light. A liquid nitrogen cooled, middle band mercury cadmium telluride detector was used for detection. Prior to

surface modification, background spectra were obtained from freshly cleaned zinc samples. The reflectance absorbance spectra shown in this work were recorded against these backgrounds.

To analyze the surface composition, X-ray photoelectron spectroscopy (XPS, Quantum 2000, Physical Electronics, Chanhassen, MN, USA) was performed at a takeoff angle of 45°, with a monochromatic Al Kα source (1486.6 eV) at a pass energy of 23.5 eV. The energy resolution used was 0.2 eV. Survey scans were performed to scan the sample for relevant elements (pass energy = 100 eV, energy step = 0.5 eV). The 1s elemental peak from carbon (285 eV) and 2p from silicon (103 eV) were measured with higher resolution (energy step 0.2 eV, pass energy 22.5 eV).

Time-of-flight secondary ion mass spectrometry (ToF-SIMS) measurements have been executed with a PHI TRIFT CE (Physical Electronics), applying a gallium ion gun on a spot size of 100 μm × 100 μm. The primary gallium ion beam was used with an energy of 15 kV, and the same ion beam was used for sputtering for 120 s on a spot size of 200 μm × 200 μm to remove ambient impurities before measuring the mass spectrum.

To determine the thickness of as synthesized polymer coatings, ellipsometry measurements were performed using a UV/visible spectroscopic ellipsometer (SE 800, Sentech Instruments GmbH, Berlin/Krailling, Germany) in the wavelength range of 400−800 nm. Measurements at three spots per sample were taken with an incident angle of 70°. Differences in ellipsometric parameters with respect to the bare zinc substrate were analyzed. Film thickness of the polymer layer on samples, regardless of modification, was obtained by fixing the refractive index of the polymer coatings to 1.5 and considering it in first approximation as wavelength independent. The value of 1.5 is close to the refractive index of PMMA of ≈1.48.[47]

2.4. Electrochemical Evaluation of Stability. Delamination experiments were performed on a commercial scanning Kelvin probe (SKP) system from KM Soft Control (Wicinski - Wicinski GbR, Wuppertal, Germany) with a 100 μm NiCr tip in humid air and nitrogen atmospheres. Before each experiment, the Kelvin probe was calibrated to the standard hydrogen electrode (SHE) against a Cu/$CuSO_4$ reference electrode. Polymer-covered zinc samples produced here were spin coated with 5 wt % poly(vinyl butyral) [PVB] in ethanol to yield a 1 μm thick polymer film. This PVB coating prevents the spreading of the electrolyte above the acrylate-coated zinc samples. Unmodified zinc substrates were spin coated with PVB, and delamination experiments were performed under similar conditions to evaluate the effect of the PVB alone. In order to initiate a cathodic delamination process, an artificial defect was created at the edge of the sample with a scalpel, and the defect was filled with 1 M KCl. The samples were subsequently introduced into a humid SKP chamber at 92% to 95% relative humidity at a temperature of around 23 °C. The progress of the delamination from was analyzed as described elsewhere.[11] The first point, which shows the potential of the intact interface, was used as the position of the delamination front. Typically, 3 to 5 samples for each given preparation were analyzed. The results presented are results of the median sample; i.e., after sorting the samples in the order of increasing stability, the sample with the middle performance was selected for presentation.

Linear polarization experiments were executed in 0.1 M KCl electrolyte by using a Voltalab Radiometer PST050 potentiostat at a scan rate of 5 mV/s. The potentiodynamic measurements were started after 1 h stabilization time of the open circuit potential (OCP) from +100 mV vs OCP anodic to −200 mV to the cathodic direction. The tested specimen had a geometric area of 0.63 cm^2. All experiments were performed in a self-made 3 electrode setup. As counter electrode, a graphite stick was used. A commercial Ag/AgCl/3 M KCl reference electrode (Metrohm, Filderstadt, Germany) served as reference electrode. All potentials are quoted here versus standard hydrogen electrode (SHE). The corrosion current densities i_{corr} were calculated from the polarization resistance R_p according to an established procedure.[48] R_p was determined as the slope of the linear polarization curve from −15 to +15 mV around E_{corr}. The Tafel slopes of the anodic and cathodic branch, β_a and β_c, respectively, were obtained from linear regions of the Tafel plots. Corrosion current densities were then calculated as[48]

$$i_{corr} = \frac{\beta_a \beta_c}{\ln(10) R_p (\beta_a + \beta_c)} \quad (1)$$

Two samples were analyzed for each given preparation.

Using a Gamry PCI4/Series G Family potentiostat (Gamry Instruments Inc.) with the same electrode setup as for linear polarization experiments, electrochemical impedance spectroscopy (EIS) was performed in the frequency range of 10^{-1} to 10^5 Hz (10 points/decade of frequency f) with 15 mV amplitude of the sinusoidal voltage modulation, at the corrosion potential. The experiments were conducted in a borate buffer solution, containing 0.2 M H_3BO_3, 0.05 M $Na_2B_4O_7$, and 0.1 M Na_2SO_4. The pH of the solution was measured as 8.4 ± 0.4. The used electrolyte provides good conductivity to perform the EIS experiments and is expected to suppress undesired formation of (sometimes protective) corrosion products. Samples were PVB coated and have been prepared as for the SKP measurements. No strong changes in the spectra have been observed after even several hours of exposure time to the solution, as water uptake starts to be decisive only after >24 h. Echem Analyst software (Gamry Instruments) has been used for fitting of the obtained data.

3. RESULTS AND DISCUSSION

3.1. Surface Modification. Zinc samples were first treated with a reactive silane coupling agent (VTS) that contains a polymerizable vinyl group. As shown in Scheme 1, the zinc surface was modified with VTS via hydrolysis of the monomer in the ethanol/water (90:10) mixture at room temperature.[49−53] The addition of water to the reaction mixture promotes the hydrolysis of methoxy groups that are present in VTS, resulting in the formation of Zn−O−Si bonds, as will be shown below.

To examine the composition of the functionalized zinc surface, IR, XP, and mass spectra were recorded. Figure 1a shows an IR spectrum of a VTS-modified zinc surface. The bands at 3020, 2965, 2921, and 2850 cm^{-1} are assigned to C−H stretching vibrations.[54] Furthermore, the peaks at 1265, 1110, 1018, and 824 cm^{-1} are modes typically observed for organic siloxane-based structures.[55] The modification of the zinc surface with VTS was further verified by conducting XPS measurements. Figure 1b shows a high-resolution XP spectrum of the Si 2p signal at the functionalized zinc sample. The presence of this Si 2p signal can be clearly identified, indicating the presence of the silicon on the zinc surface. To further verify the presence of chemical bonding between zinc and the silane coupling agent, ToF-SIMS analysis was performed. Initially, the top layer of VTS was sputtered away by ion etching, to analyze the interfacial region between the native oxide on zinc and the organosilane. In the region between organic film and native oxide, the fragment $ZnOSi^+$ was detected, as shown in Figure 1c. The ion pattern of the fragment $ZnOSi^+$ should reflect the isotopic abundance of the elements present; the observed distribution is in close agreement to the calculated distribution.[56] Deviations at the peaks of species with lower abundance at ≈109 and ≈111 amu are attributed to contributions of organic fragments to the totally measured count rate. The presence of the $ZnOSi^+$ fragment is an indication of the formation of a covalent bond between organosilane and the native oxide on zinc.[56] It is known that hydrolyzed alkoxysilanes may react with each other to form a dense polymeric film on the surface,[50,57] while care is needed to ensure the formation of a monolayer.[46] Here, ellipsometric

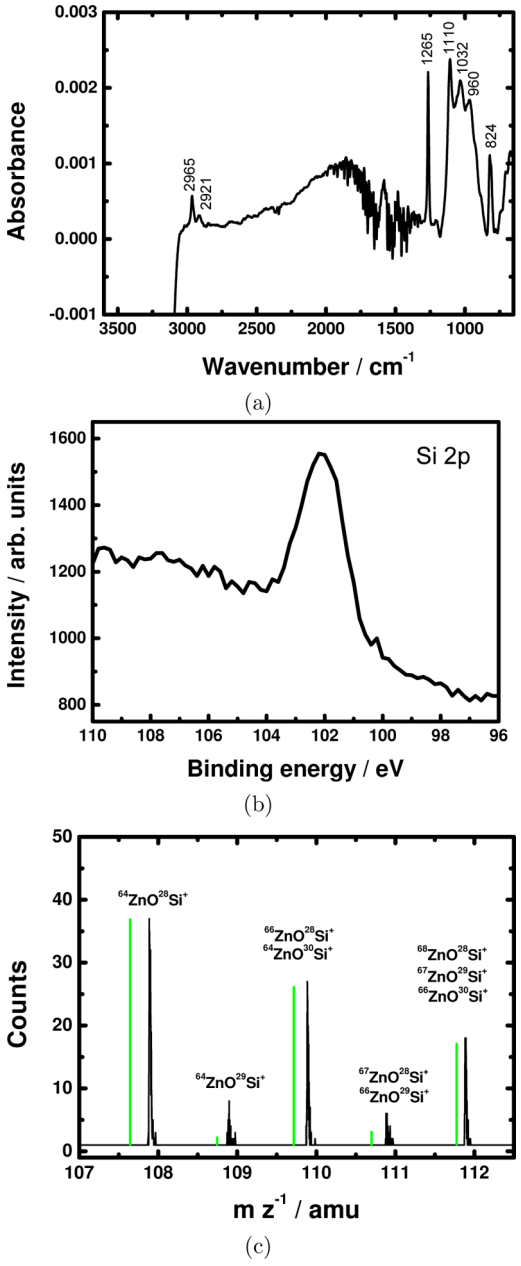

Figure 1. (a) IR spectrum of VTS-modified zinc. (b) Si 2p region of the XP spectrum of VTS-modified zinc. The presence of the signal confirms the presence of silane on the surface. (c) SIMS showing the isotope distribution of $ZnOSi^+$ fragments from the surface of VTS-modified zinc. Expected isotope distribution is shown as vertical lines (green |) ca. 0.3 amu below the experimental peak.

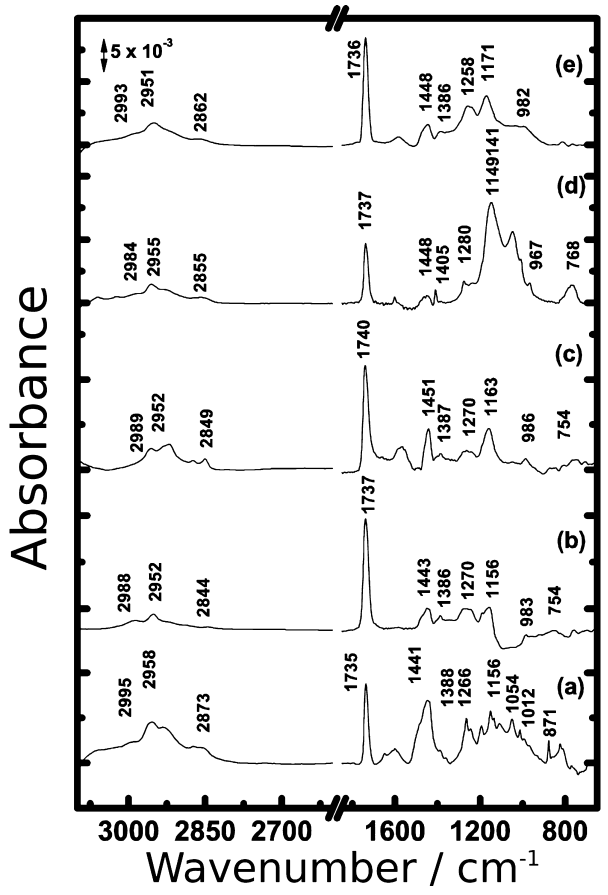

Figure 2. IR spectra of different covalently bound polymer coatings on zinc, (a) PMMA without cross-linker, (b) PMMA + 25% EDA, (c) PMMA + 50% EDA, (d) PMMA + 25% HDA, and (e) PMMA + 50% HDA.

analysis yields a thickness of 2−3 nm of the silane layers, clearly above monolayer coverage, but still significantly below 10 nm.

Formation of a covalent bond between PMMA and the VTS-modified surface was achieved by performing a thermally initiated polymerization of methyl methacrylate in the presence of the modified zinc substrate with AIBN as initiator (see Scheme 1). Two fractions of PMMA after the copolymerization reaction were obtained, a covalently surface-bound fraction and a fraction without covalent bond to the surface. The fraction that is physisorbed on the surface was washed with excess toluene to remove the nonbounded polymer. Figure 2a shows the measured IR spectra after copolymerization. Appearance of characteristic C═O stretching mode as a band at 1735−1740 cm^{-1} is an indication of the presence of an acrylate bound to the zinc sample.[54] In addition to copolymerization with the monofunctional monomer MMA, polymerization was also carried out in the presence of bifunctional acrylates with different chain length and different molar fractions (25% and 50%). The presence of such monomers in the copolymerization results in films consisting of cross-linked polymers. Figure 2b−e shows the IR spectra of polymer films prepared in the presence of cross-linker. Furthermore, XP spectra (Figure 3) of polymer-modified samples show the expected C 1s and O 1s peaks. The high resolution C 1s spectrum can be decomposed into four distinct peaks at 284.8, 285.4, 286.4, and 288.8 eV that originate from aliphatic carbon, **C**−COO, **C**−O, and **C**OO, respectively.[58] The fraction of **C**OO was quantified to be in the range of 8% and 17% of the total carbon, without a clear trend between the different polymers, but with high repeatability between different samples of the same polymer. This fraction is slightly lower than expected (for HDA homopolymers 16.7%, for pure PMMA 20%, and for EDA homopolymers 25%). The fraction detected by XPS is, however, also affected by the distribution of the elements inside the thin films. The results here may indicate that carboyxl groups may be enriched inside the film, and oxygen-poor parts of the polymer chains may be present directly at the surface. Initiator fragments inside the film may also lower the **C**OO fraction. In all samples after polymerization, the Si 2p peak remains centered at 102 eV, as shown for the VTS-modified surface in Figure 1b. This peak

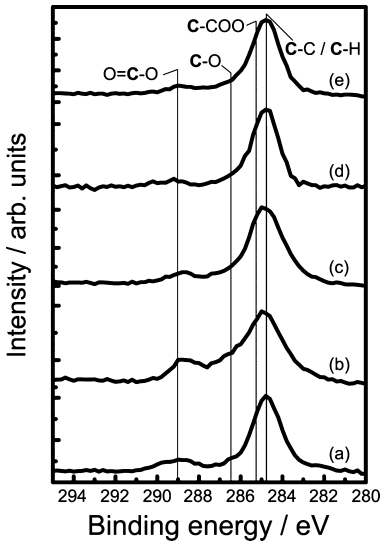

Figure 3. C 1s region of the XP spectrum of zinc with different polymer coatings, (a) PMMA without cross-linker, (b) PMMA + 25% EDA, (c) PMMA + 50% EDA, (d) PMMA + 25% HDA, and (e) PMMA + 50% HDA. The line represents the respective peak position for the atom shown in bold on its label.[58]

position is typical for organosilanes,[58] indicating that these structures are still present in an unmodified form after polymerization. In the XP spectra, Zn peaks are absent except for films with a thickness <10 nm, confirming a full coverage of the zinc with polymer on the level of XPS sensitivity.

The thickness of the obtained polymer films was analyzed by ellipsometry. As shown in Table 1, an increase in the cross-linker fraction results in the reduction of polymer film thickness. This observation is tentatively attributed to a higher rate of quenching of the propagation reaction in case larger amounts of cross-linker are used.[59] Ellipsometric spectra could be well-described by a simple ambient−film−substrate model, which confirms that the films are not inhomogeneous on the length scale of several tens of nanometers.

Table 1. Polymer Film Thickness Obtained from Ellipsometric Measurements for PMMA Samples with Different Cross-Linker Ratios

sample	thickness/nm
no cross-linker	25 ± 5
25% EDA	12 ± 2
50% EDA	9 ± 2
25% HDA	14 ± 3
50% HDA	12 ± 3

3.2. Model Corrosion Experiments. In order to study the stability of these produced silane-bonded PMMA coatings against cathodic delamination, the propagation of a delamination front from a defect filled with 1 M KCl was monitored by scanning Kelvin probe measurements. Figure 4 shows the SKP potential profile recorded on spin coated PVB, as well as on covalently bound PMMA. Scans were obtained by scanning along the surface from the artificial defect and show the recorded potential as a function of distance from the defect for different times. In the initial stages of the experiment, the SKP measures the potential of an intact (i.e., noncorroded) polymer/oxide/metal interface all over the sample. However,

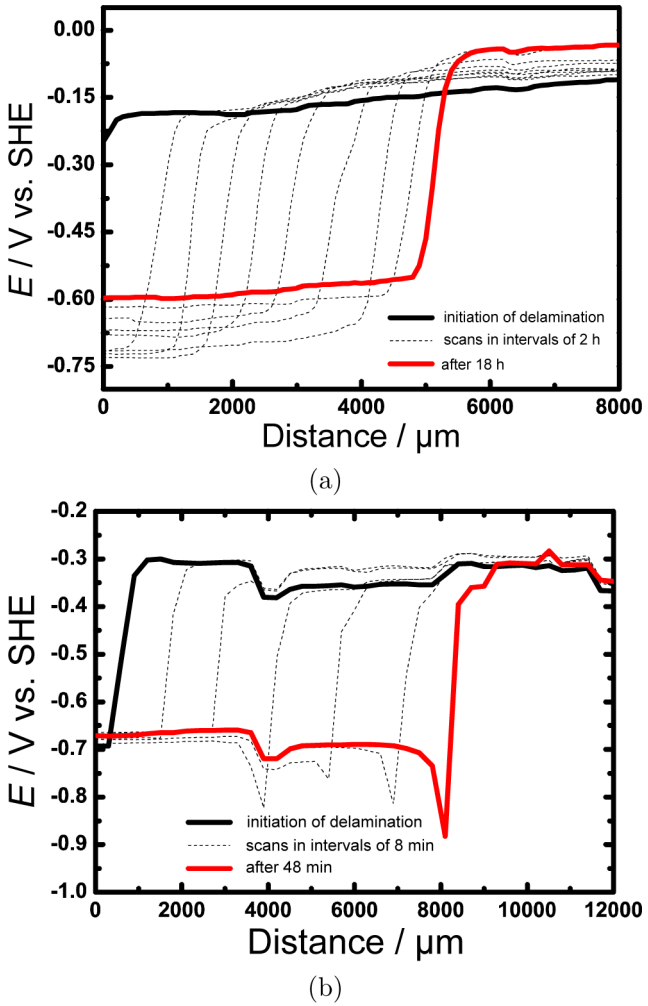

Figure 4. Scanning Kelvin probe delamination profile of (a) covalently bound PMMA on zinc and (b) weakly bound PVB used for reference purposes, both in air.

with time, cathodic delamination is initiated in a humid air atmosphere on both samples as shown in Figure 4. Consequently, during passage of a delamination front, two distinct potential levels are observed.[11] The more negative potential (≈−0.7 V) indicates actively corroding zinc in the region where the polymer is already delaminated, while the more positive potential (≈−0.2 V) indicates an intact polymer/metal interface.[11] Between these two potentials, a sharp transition region can be observed, which is the position of the delamination front.[11]

The progress of the delamination front with time t is plotted in Figure 5 for several coatings. Plotting the same results on a double logarithmic scale (Figure 5a) enables one to determine the exponent α of the time dependence. While for diffusion controlled processes the position d of the delamination front travels as $d \sim t^{1/2}$ ($\alpha = 1/2$),[9] a time dependence as $d \sim t^1$ ($\alpha = 1$) is expected if a first-order reaction is rate-determining. Alternatively, $d \sim t^1$ may indicate migration in a constant static electric field. Here, exponents $\alpha \approx 1$ are found, with maximum 5% deviation for all except one portion of the curve, which will be discussed below. Hence, the delamination rate r was determined from the slope of a linear fit in Figure 5b. The rates for different samples are shown in Table 2. Figure 5b shows that the progress of the delamination front is inhibited on zinc

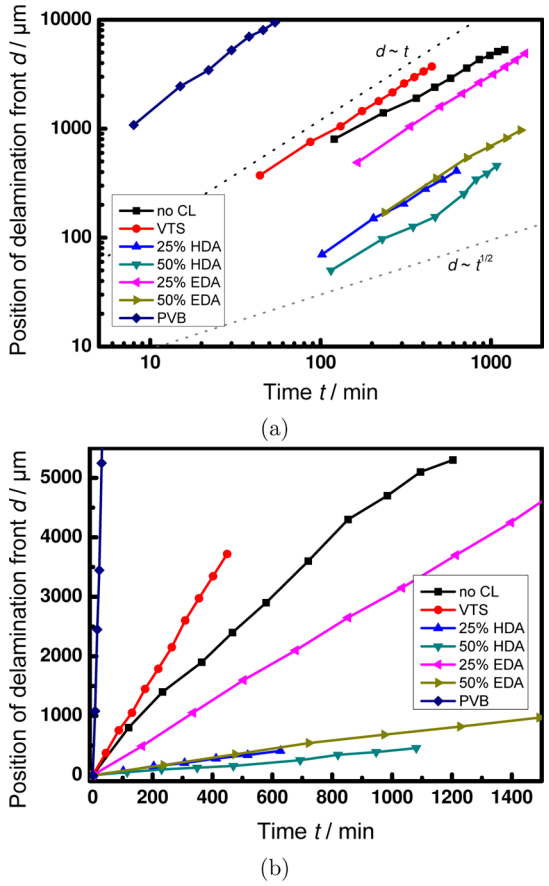

Figure 5. Comparison of the delamination rates for polymer coatings with different cross-linker amounts (a) on a double logarithmic scale and (b) on a linear scale. In plot (a), two dotted lines show the expected slopes for $d \sim t$ and $d \sim t^{1/2}$, as indicated in the graph. The delamination rates resulting from linear fits, averaged over three samples, are shown in Table 2.

Table 2. Delamination Rates and Standard Deviations for the Different Samples, Based on Linear Fits of Plots as in Figure 5b[a]

sample	delamination rate/mm h^{-1}
pure PVB	11.2 ± 0.5
VTS	0.52 ± 0.03
no cross-linker	0.27 ± 0.02
25% EDA	0.22 ± 0.02
50% EDA	0.042 ± 0.004
25% HDA	0.039 ± 0.003
50% HDA	0.028 ± 0.004

[a]All samples were covered with PVB, as explained in the Experimental Section.

substrate modified with covalently bound PMMA without cross-linker (r = 0.27 ± 0.02 mm h^{-1}), compared to the reference sample with spin-coated PVB (r = 11.2 ± 0.5 mm h^{-1}) and spin-coated PVB on VTS-modified zinc (r = 0.52 ± 0.03 mm h^{-1}). When changing from a humid air atmosphere to humid nitrogen, no cathodic delamination was observed. In this case, the potential remained at the potential of the intact polymer/metal interface. (Attempts to produce PMMA films by spin coating, which were not covalently linked but have a thickness comparable to the thickness of the synthesized layers, failed.)

In order to gain further insight into the effect of network chain length and degree of cross-linking on the stability of these coatings against corrosion in general and against cathodic delamination in particular, additional coatings were synthesized on VTS-modified zinc substrates with two different cross-linker chain lengths. The different molar ratios empolyed should result in a different degree of cross-linking. Delamination was monitored by SKP, and the delamination rates obtained are included in Figure 5. In one case of the cross-linked samples, namely, in the case of coatings containing 50% HDA cross-linker, a t^1 behavior is found initially, which at larger times changes to $t^{1/2}$. Such a transition is observed only for this particular type of sample. Overall, the results show a higher rate of delamination for EDA-cross-linked samples compared to HDA-cross-linked samples. That is, polymer coatings with a shorter cross-linker chain length delaminate faster than coatings with a longer chain between the two polymerizable functional groups of the cross-linker. Further, an increase in the amount of cross-linker leads to a decrease in the delamination rate. EDA-cross-linked samples delaminate, however, at a similar rate than non-cross-linked samples.

Furthermore, investigation of the samples after a delamination experiment with scanning electron microscopy reveals the growth of crystalline ZnO corrosion products. The growth of zinc oxide/hydroxide structures after cathodic delamination has been shown in the past.[11,39]

The corrosion resistance of the different coatings was also evaluated by performing linear polarization experiments. Typical Tafel plots obtained for bare zinc and coated zinc are shown in Figure 6. (It must be noted that, compared to the SKP experiments, no PVB coating was present for these experiments.) Corresponding corrosion current rates were calculated from the polarization resistance[48] and are tabulated in Table 3. The highest values of corrosion current were naturally recorded for bare, uncoated zinc. Consequently, zinc oxidation rates (from oxide formation and dissolution) as well as the accompanying cathodic reaction, most likely the oxygen reduction reaction in this system, are the highest for pure zinc. Overall corrosion currents are lower for coated zinc samples, showing that indeed the coatings have the expected corrosion-inhibiting effect. The comparison of the corrosion currents from the different samples (Table 3) shows that all cross-linked coatings show lower corrosion currents than coatings without cross-linking. The sample with the lowest overall corrosion current is the same one that shows the lowest delamination rate. However, the difference between EDA and HDA is not clearly visible in the corrosion currents. Both coatings also inhibit the dissolution as expected, which is shown in the lower currents in the anodic branch of the plots in Figure 6.

The typical Bode plots of the investigated materials after 2 h of immersion are given in Figure 7. The 50% HDA cross-linked polymer indicates a prevailing capacitive behavior. The corresponding EIS spectrum shows only one time constant after 2 h of immersion. However, in the case of the other samples, the phase angle is starting to decrease at lower frequencies, a consequence of the electrolyte ingress into the polymer. As a consequence of the penetrating solution, electrochemical reactions can take place at the metal surface, resulting in the presence of a second time constant in the Bode plots.[60] The first process at high frequencies can be attributed to the coating capacitance and resistance. The second process at low frequencies can be related to the charge transfer resistance and the electrical double-layer capacitance at the

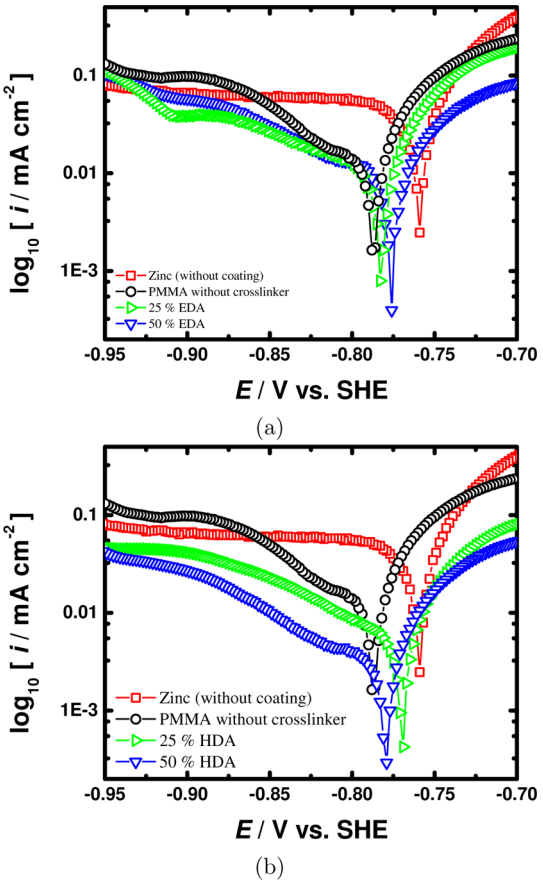

Figure 6. Polarization curves in the form of Tafel plots in 0.1 M KCl for zinc with different coatings, (a) with EDA cross-linker and (b) with HDA cross-linker.

Table 3. Corrosion Current Densities i_{corr} for Differently Coated Samples in 0.1 M KCl[a]

sample	β_a/mV dec^{-1}	β_c/mV dec^{-1}	R_p/Ω cm^2	i_{corr}/μA cm^{-2}
zinc uncoated	104 ± 4	176 ± 3	317 ± 15	89 ± 5
no cross-linker	105 ± 4	196 ± 8	780 ± 60	38 ± 4
25% EDA	43 ± 3	161 ± 2	860 ± 30	17 ± 1
50% EDA	54 ± 2	168 ± 3	1120 ± 30	15.8 ± 0.7
25% HDA	62 ± 2	150 ± 3	1560 ± 50	12.2 ± 0.6
50% HDA	58 ± 2	137 ± 3	4200 ± 200	4.2 ± 0.3

[a]dec = decade of current. "no cross-linker" refers to non-cross-linked PMMA.

metal/solution interface.[60] Moreover, on the basis of the decrease of the impedance modulus at the lowest frequencies (10^{-1} Hz), a comparison of the protective properties of the selected systems can be made, via the charge transfer resistance. There is a tendency for the more hydrophobic HDA cross-linker to grant better protection from water ingress than the EDA cross-linker. Higher cross-linker concentrations also slow down the penetration of the electrolyte to the metal surface.

Plasma polymers are ultrathin polymer films which are typically highly cross-linked. The charge transfer/polarization resistances found here for coatings by free radical polymerization are in a similar order of magnitude compared with literature data on plasma polymers.[61] The slowest delamination rates found here are of the same order as published results for

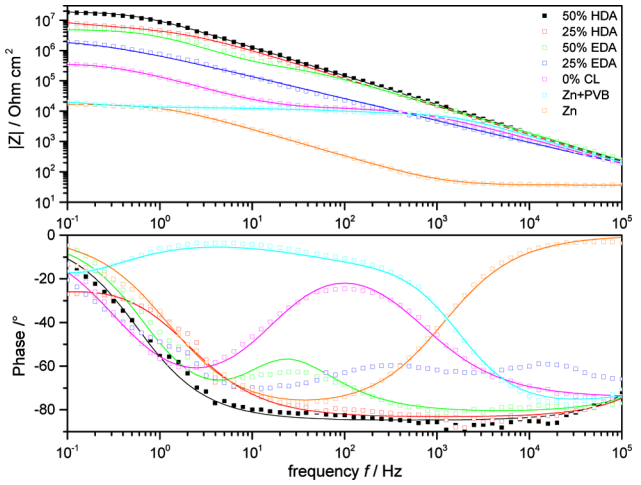

Figure 7. Bode plots (top: modulus of impedance |Z|; bottom: phase) for the selected polymer systems as indicated in the graph after 2 h of immersion in borate buffer. The straight lines represent the fitted curves of the corresponding sample.

plasma polymers on steel with even lower electrolyte concentration.[30]

3.3. Discussion of the Chemistry of Cathodic Delamination. First, it is obvious that the presence of a coating on metallic zinc reduces the corrosion rates, as it inhibits interfacial electron transfer reactions through blocking transport paths and active sites. Second, a covalently bound coating delaminates considerably slower than a coating which is attached to the surface by van der Waals forces only. It is known that modification of oxide-covered metal surfaces with covalently bound polymers inhibits the oxygen reduction reaction at the polymer/metal interface as a result the strong chemical bond.[62−64]

The linear dependence of the delamination front location from the experiment time shows that diffusion (e.g., of oxygen or water through the coating) is not rate limiting.[9] Indeed, for low oxygen partial pressure, the contribution of ion diffusion to overall transport was reported to be overestimated.[17] Consequently, the differences observed for delamination rates and corrosion currents between the cross-linked polymer coatings cannot be explained by differences in transport through the thin polymer films. Likewise, the relatively small differences between the polymer coating thicknesses cannot explain the observed differences, as the thinner coatings with high molar ratios of cross-linkers show lower corrosion currents than the slightly thicker coatings.

The overall amount of hydrophobic groups is one factor contributing to the observed differences between the coatings. Large fractions of HDA in the monomer solution lead to the presence of a large fraction of hydrophobic alkyl chains in the final polymer. EDA as cross-linker on the other hand does not significantly alter hydrophilicity of the polymer layers compared to PMMA. Hydrophobic polymer layers cannot take up as much water as less hydrophobic coatings. Lower availability of the solvent water during the corrosion process is decreasing the corrosion rate and the delamination rate. The coating, which is expected to be the most hydrophobic, changes to a transport-controlled delamination mechanism at longer exposure.

The behavior of the coatings in linear polarization experiments and in delamination experiments is not the same. Coatings without cross-linker show similar delamination rates

as EDA-cross-linked coatings, while their corrosion currents are twice as high. As cross-linked coatings block transport routes in between different polymer chains, they decrease the corrosion current but not the delamination rate. Delamination rates do overall roughly follow the same trends as observed for the low-frequency impedance modulus, which reflects the charge transfer resistance.

The observed t^1-delamination kinetics may be determined by migration of ions in a constant electrostatic potential gradient or by a first-order chemical reaction. In migration in the electric field, ion flux is proportional to the electric field gradient (e.g., ref 37). When comparing the delamination curves (e.g., shown in Figure 4), it becomes obvious that the potential difference between active and nonactive region is very similar for all polymers. With the lateral resolution used here, the distance above which the potential drop is observed is also quite similar for the different samples. Hence, the differences in delamination rate between the different samples caused by migration in the electric field alone should be rather small. We therefore focus on the discussion of the chemical reactions being responsible for the observed differences between the coatings.

Considering cathodic delamination, two types of reactions could be rate determining, either the oxygen reduction reaction (ORR), which drives the delamination front, or the deadhesion process, which involves breaking of covalent bonds in the reactions here. It is hard to see why the rate of the ORR should depend on the amount of cross-linker present in the preparation. Instead, the ORR rate, as any rate of an electron transfer reaction, is a sensitive probe of the state of the interface, especially of defects in the layers, i.e., the free metal surface which is available to the electron transfer reaction. While it is possible that the presence of the cross-linker in the copolymerization reaction modifies the interface, it is less likely. All surfaces were subjected to identical treatments before polymerization, so the metal(oxide)/silane interface is supposed to be identical.

In the actual deadhesion process, several processes could potentially occur. It is known that the hydoxide as reaction product of the ORR leads to strongly alkaline conditions in the vicinity of the delamination front.[11] Hydroxide could be involved in a number of follow up reactions: (a) in the alkaline dissolution of zinc oxide under hydroxozincate formation according to

$$ZnO + 2OH^- + H_2O \rightarrow Zn(OH)_4^{2-} \quad (2)$$

or (b) in the alkaline hydrolysis of Si−O bonds under silicate formation according to

$$R^{(1)}\text{–}Si(\text{–}OR^{(2)})_3 + 3H_2O \xrightarrow{OH^-} R^{(1)}Si(OH)_3 + 3R^{(2)}OH \quad (3)$$

Both reactions are possible at pH > 11.[65] Both dissolution of ZnO and hydrolysis of Si−O bonds are not expected to be affected by the presence of cross-linked structures in the polymer film. In both cases, the inorganic part of the metal/polymer interface will dissolve. A further degradation reaction is an alkaline ester hydrolysis of the PMMA under formation of carboxylate and alcohol according to

$$R^{(1)}\text{–}COO\text{–}R^{(2)} + OH^- \rightarrow R^{(1)} - COO^- + R^{(2)}OH \quad (4)$$

This reaction does, however, not lead to a breakage of the polymer main chain and, hence, not to deadhesion of the complete coating. Alkaline ester hydrolysis would, however, affect the cross-linking, as both cross-linkers link polymer chains via ester bonds. As an alternative to processes involving OH^-, radical reactions are other candidates which could lead to the deadhesion of the polymer films. Radical intermediates have been shown to occur in the ORR.[66,67] Here, only a radical reaction can explain all the results without involvement of a complex coupling of polymer degradation and, e.g., zinc oxide dissolution. Previous reports have shown a decrease in delamination rate in the presence of radical scavengers.[68]

The situation encountered in this work is significantly different from the situation in a previous work, where a larger cross-linker amount was found to lead to higher delamination rates in latex polymers because of the increase in interfacial free volume.[69] Interfacial free volume can form in a significant amount in coatings, which form by coalescence of latex particles, but is less likely to occur in a significant amount in coatings prepared directly by free radical polymerization, as is used here. Especially, if interfacial free volume forms, its relation to the cross-linking is not straightforward.

4. SUMMARY AND CONCLUSIONS

Free radical copolymerization of dissolved and surface-bound monomers has been used to synthesize PMMA coatings with thicknesses in the order of 10−20 nm on the industrially relevant metal zinc. Adding certain amounts of cross-linkers enables a systematic variation of the degree of cross-linking in the resulting coatings. The coatings prepared here are covalently linked to the base metal via organosilanes. Such coatings show a larger resistance toward cathodic delamination than coatings bound exclusively via van der Waals interactions. The delamination rate decreases to <1/10 only by introducing covalent bonds to the base metal. Introduction of cross-linkers further slows down delamination, with another factor of ∼10 between non-cross-linked PMMA and samples with 50% cross-linker. Comparing the two cross-linkers used in this study, the more hydrophobic HDA yields the lowest delamination rates of all samples investigated in this study, 0.028 ± 0.004 mm h^{-1}. The coatings prepared here via a wet chemical process lead to similar delamination rates, corrosion current densities, and charge transfer resistance values as plasma polymers prepared by a gas phase process.

Delamination rates are reaction-controlled for the systems investigated here, as shown by the t^1 dependence. In particular, diffusion limitation can be excluded, as this would lead to a $t^{1/2}$ dependence. Because delamination rates depend on the presence of cross-linkers and the degree of cross-linking, the rate-limiting reaction must be related to the polymer of the coating. This observation rules out alkaline zinc oxide dissolution and siloxane bond hydrolysis as the sole reactions leading to deadhesion. Radical reactions as side reactions of the oxygen reduction can explain the observed trends in the delamination rate with variation of interface composition. A delamination mechanism not centered around radical reactions needs to involve an unlikely coupling by an unknown mechanism between alkaline dissolution of inorganic surface linkages and polymer degradation.

AUTHOR INFORMATION

Corresponding Author

*E-mail: aerbe@arcor.de; a.erbe@mpie.de. Phone: +49 (0)211 6792890. Fax: +49 (0)211 6792218.

Notes

The authors declare no competing financial interest.

■ ACKNOWLEDGMENTS

D.I. acknowledges a scholarship from the International Max Planck Research School for Surface and Interface Engineering in Advanced Materials (IMPRS-SurMat). A.A. and A.E. acknowledge support from the DFG (Deutsche Forschungsgemeinschaft) by grant number ER 601/3-1 within the Priority Program 1640 "Joining by plastic deformation". This work is supported by the Cluster of Excellence RESOLV (EXC 1069) funded by the Deutsche Forschungsgemeinschaft. The authors thank Prof. M. Stratmann for continuous support and fruitful discussion.

■ REFERENCES

(1) Davis, J. R. *Corrosion - Understanding the Basics*; ASM International: Materials Park, OH, 2000.
(2) McMurray, H.; Williams, G. In *Shreir's Corrosion*; Cottis, B., Graham, M., Lindsay, R., Lyon, S., Richardson, T., Scantlebury, D., Stott, H., Eds.; Elsevier: Oxford, 2010; Chapter 2.14, pp 988−1004.
(3) Grundmeier, G.; Alda, S. In *Encyclopedia of Electrochemistry*; Bard, A., Stratmann, M., Frankel, G., Eds.; Wiley-VCH: Weinheim, Germany, 2007; Vol. *4*; Chapter Corrosion Protection by Organic Coatings, pp 500−566.
(4) Grundmeier, G.; Stratmann, M. Adhesion and De-Adhesion Mechanisms at Polymer/Metal Interfaces: Mechanistic Understanding Based on in Situ Studies of Buried Interfaces. *Annu. Rev. Mater. Res.* **2005**, *35*, 571−615.
(5) By "metal(oxide)/polymer interface", we designate the interfacial region between a metal that is typically covered by a native oxide and a polymer.
(6) Amirudin, A.; Thierry, D. Corrosion Mechanisms of Phosphated Zinc Layers on Steel as Substrates for Automotive Coatings. *Prog. Org. Coat.* **1996**, *28*, 59−75.
(7) Stratmann, M.; Wolpers, M.; Streckel, H.; Feser, R. Use of a Scanning-Kelvinprobe in the Investigation of Electrochemical Reactions at the Metal/Polymer Interface. *Ber. Bunsen-Ges.* **1991**, *95*, 1365−1375.
(8) Leng, A.; Streckel, H.; Stratmann, M. The Delamination of Polymeric Coatings from Steel. Part 1: Calibration of the Kelvinprobe and Basic Delamination Mechanism. *Corros. Sci.* **1998**, *41*, 547−578.
(9) Leng, A.; Streckel, H.; Stratmann, M. The Delamination of Polymeric Coatings from Steel. Part 2: First Stage of Delamination, Effect of Type and Concentration of Cations on Delamination, Chemical Analysis of the Interface. *Corros. Sci.* **1998**, *41*, 579−597.
(10) Leng, A.; Streckel, H.; Hofmann, K.; Stratmann, M. The Delamination of Polymeric Coatings from Steel. Part 3: Effect of the Oxygen Partial Pressure on the Delamination Reaction and Current Distribution at the Metal/Polymer Interface. *Corros. Sci.* **1998**, *41*, 599−620.
(11) Fürbeth, W.; Stratmann, M. The Delamination of Polymeric Coatings from Electrogalvanised Steel - A Mechanistic Approach. Part 1: Delamination from a Defect with Intact Zinc Layer. *Corros. Sci.* **2001**, *43*, 207−227.
(12) Fürbeth, W.; Stratmann, M. The Delamination of Polymeric Coatings from Electrogalvanized Steel - A Mechanistic Approach. Part 2: Delamination from a Defect down to Steel. *Corros. Sci.* **2001**, *43*, 229−241.
(13) Maeda, S. Surface Chemistry of Galvanized Steel Sheets Relevant to Adhesion Performance. *Prog. Org. Coat.* **1996**, *28*, 227−238.
(14) Awaja, F.; Gilbert, M.; Kelly, G.; Fox, B.; Pigram, P. J. Adhesion of Polymers. *Prog. Polym. Sci.* **2009**, *34*, 948−968.
(15) Rangwalla, H.; Dhinojwala, A. Probing Hidden Polymeric Interfaces Using IR-Visible Sum-Frequency Generation Spectroscopy. *J. Adhes.* **2004**, *80*, 37−59.
(16) Zhang, C.; Myers, J. N.; Chen, Z. Elucidation of Molecular Structures at Buried Polymer Interfaces and Biological Interfaces Using Sum Frequency Generation Vibrational Spectroscopy. *Soft Matter* **2013**, *9*, 4738−4761.
(17) Posner, R.; Santa, M.; Grundmeier, G. Wet-and Corrosive De-Adhesion Processes of Water-Borne Epoxy Film Coated Steel I. Interface Potentials and Characteristics of Ion Transport Processes. *J. Electrochem. Soc.* **2011**, *158*, C29−C35.
(18) Taheri, P.; Ghaffari, M.; Flores, J.; Hannour, F.; de Wit, J.; Mol, J.; Terryn, H. Bonding Mechanisms at Buried Interfaces between Carboxylic Polymers and Treated Zinc Surfaces. *J. Phys. Chem. C* **2013**, *117*, 2780−2792.
(19) Santa, M.; Posner, R.; Grundmeier, G. Wet-and Corrosive De-Adhesion Processes of Water-Borne Epoxy Film Coated Steel II. The Influence of γ-Glycidoxypropyltrimethoxysilane as an Adhesion Promoting Additive. *J. Electrochem. Soc.* **2011**, *158*, C36−C41.
(20) Tran, Y.; Auroy, P. Synthesis of Poly(Styrene Sulfonate) Brushes. *J. Am. Chem. Soc.* **2001**, *123*, 3644−3654.
(21) Sofia, S. J.; Premnath, V.; Merrill, E. W. Poly(Ethylene Oxide) Grafted to Silicon Surfaces: Grafting Density and Protein Adsorption. *Macromolecules* **1998**, *31*, 5059−5070.
(22) Luzinov, I.; Julthongpiput, D.; Malz, H.; Pionteck, J.; Tsukruk, V. V. Polystyrene Layers Grafted to Epoxy-Modified Silicon Surfaces. *Macromolecules* **2000**, *33*, 1043−1048.
(23) Barbey, R.; Lavanant, L.; Paripovic, D.; Schüwer, N.; Sugnaux, C.; Tugulu, S.; Klok, H.-A. Polymer Brushes via Surface-Initiated Controlled Radical Polymerization: Synthesis, Characterization, Properties, and Applications. *Chem. Rev.* **2009**, *109*, 5437−5527.
(24) Meyer, T.; Spange, S.; Hesse, S.; Jäger, C.; Bellmann, C. Radical Grafting Polymerization of Vinylformamide with Functionalized Silica Particles. *Macromol. Chem. Phys.* **2003**, *204*, 725−732.
(25) Laible, R.; Hamann, K. Formation of Chemically Bound Polymer Layers on Oxide Surfaces and Their Role in Colloidal Stability. *Adv. Colloid Interface Sci.* **1980**, *13*, 65−99.
(26) Zhang, B.; Hu, N.; Wang, Y.; Wang, Z.; Wang, Y.; Kong, E. S.; Zhang, Y. Poly(Glycidyl Methacrylates)-Grafted Zinc Oxide Nanowire by Surface-Initiated Atom Transfer Radical Polymerization. *Nano-Micro Lett.* **2010**, *2*, 285−289.
(27) Prucker, O.; Rühe, J. Mechanism of Radical Chain Polymerizations Initiated by Azo Compounds Covalently Bound to the Surface of Spherical Particles. *Macromolecules* **1998**, *31*, 602−613.
(28) Prucker, O.; Rühe, J. Synthesis of Poly(Styrene) Monolayers Attached to High Surface Area Silica Gels through Self-Assembled Monolayers of Azo Initiators. *Macromolecules* **1998**, *31*, 592−601.
(29) Liu, H.; O'Mahony, C. T.; Audouin, F.; Ventura, C.; Morris, M.; Heise, A. Random Poly(methyl methacrylate-co-styrene) Brushes by ATRP to Create Neutral Surfaces for Block Copolymer Self-Assembly. *Macromol. Chem. Phys.* **2012**, *213*, 108−115.
(30) Grundmeier, G.; Stratmann, M. Plasma Polymerization - A New and Promising Way for the Corrosion Protection of Steel. *Mater. Corros.* **1998**, *49*, 150−160.
(31) Delattre, J. L.; dAgostino, R.; Fracassi, F. Plasma-Polymerized Thiophene Films for Enhanced Rubber-Steel Bonding. *Appl. Surf. Sci.* **2006**, *252*, 3912−3919.
(32) Vasudev, M. C.; Anderson, K. D.; Bunning, T. J.; Tsukruk, V. V.; Naik, R. R. Exploration of Plasma-Enhanced Chemical Vapor Deposition as a Method for Thin-Film Fabrication with Biological Applications. *ACS Appl. Mater. Interfaces* **2013**, *5*, 3983−3994.
(33) Li, P.; Li, L.; Wang, W.; Jin, W.; Liu, X.; Yeung, K. W.; Chu, P. K. Enhanced Corrosion Resistance and Hemocompatibility of Biomedical NiTi Alloy by Atmospheric-Pressure Plasma Polymerized Fluorine-Rich Coating. *Appl. Surf. Sci.* **2014**, *297*, 109−115.
(34) Posner, R.; Wapner, K.; Stratmann, M.; Grundmeier, G. Transport Processes of Hydrated Ions at Polymer/Oxide/Metal Interfaces: Part 1. Transport at Interfaces of Polymer Coated Oxide Covered Iron and Zinc Substrates. *Electrochim. Acta* **2009**, *54*, 891−899.
(35) Posner, R.; Titz, T.; Wapner, K.; Stratmann, M.; Grundmeier, G. Transport Processes of Hydrated Ions at Polymer/Oxide/Metal

Interfaces: Part 2. Transport on Oxide Covered Iron and Zinc Surfaces. *Electrochim. Acta* **2009**, *54*, 900−908.
(36) Sørensen, P.; Dam-Johansen, K.; Weinell, C.; Kiil, S. Cathodic Delamination: Quantification of Ionic Transport Rates Along Coating-Steel Interfaces. *Prog. Org. Coat.* **2010**, *68*, 70−78.
(37) Montoya, R.; Garca-Galván, F.; Jiménez-Morales, A.; Galván, J. A Cathodic Delamination Study of Coatings with and without Mechanical Defects. *Corros. Sci.* **2014**, *82*, 432−436.
(38) Khun, N.; Frankel, G. Effects of Surface Roughness, Texture and Polymer Degradation on Cathodic Delamination of Epoxy Coated Steel Samples. *Corros. Sci.* **2013**, *67*, 152−160.
(39) Iqbal, D.; Moirangthem, R. S.; Bashir, A.; Erbe, A. Study of Polymer Coating Delamination Kinetics on Zinc Modified with Zinc Oxide of Different Morphologies. *Mater. Corros.* **2014**, *65*, 370−375.
(40) Sørensen, P.; Dam-Johansen, K.; Weinell, C.; Kiil, S. Cathodic Delamination of Seawater-Immersed Anticorrosive Coatings: Mapping of Parameters Affecting the Rate. *Prog. Org. Coat.* **2010**, *68*, 283−292.
(41) Nazarov, A.; Olivier, M.-G.; Thierry, D. SKP and FT-IR Microscopy Study of the Paint Corrosion De-Adhesion from the Surface of Galvanized Steel. *Prog. Org. Coat.* **2012**, *74*, 356−364.
(42) Huang, M.-W.; Allely, C.; Ogle, K.; Orazem, M. E. A Mathematical Model for Cathodic Delamination of Coated Metal Including a Kinetic pH-Porosity Relationship. *J. Electrochem. Soc.* **2008**, *155*, C279−C292.
(43) Paliwoda-Porebska, G.; Stratmann, M.; Rohwerder, M.; Potje-Kamloth, K.; Lu, Y.; Pich, A.; Adler, H.-J. On the Development of Polypyrrole Coatings with Self-Healing Properties for Iron Corrosion Protection. *Corros. Sci.* **2005**, *47*, 3216−3233.
(44) Vimalanandan, A.; Lv, L.-P.; Tran, T. H.; Landfester, K.; Crespy, D.; Rohwerder, M. Redox-Responsive Self-Healing for Corrosion Protection. *Adv. Mater.* **2013**, *25*, 6980−6984.
(45) Saikia, P. J.; Lee, J. M.; Lee, B. H.; Choe, S. Reversible Addition Fragmentation Chain Transfer Mediated Dispersion Polymerization of Styrene. *Macromol. Symp.* **2007**, *248*, 249−258.
(46) Niehoff, P.; Ebbinghaus, P.; Keil, P.; Erbe, A. Monolayer Formation of Octyltrimethoxysilane and 7-Octenyltrimethoxysilane on Silicon(100) Covered with Native Oxide. *Appl. Surf. Sci.* **2012**, *258*, 3191−3196.
(47) Brandrup, J.; Immergut, E. H.; Grulke, E. A. *Polymer Handbook*, 4th Ed.; Wiley: New York, 1999.
(48) Stern, M.; Geary, A. L. Electrochemical Polarization: I. A Theoretical Analysis of the Shape of Polarization Curves. *J. Electrochem. Soc.* **1957**, *104*, 56−63.
(49) Mittal, K. *Silanes and Other Coupling Agents*; VSP: Utrecht, The Netherlands, 1992.
(50) Bressy, C.; Ngo, V. G.; Ziarelli, F.; Margaillan, A. New Insights into the Adsorption of 3-(Trimethoxysilyl) Propylmethacrylate on Hydroxylated ZnO Nanopowders. *Langmuir* **2012**, *28*, 3290−3297.
(51) Posthumus, W.; Magusin, P.; Brokken-Zijp, J.; Tinnemans, A.; Van der Linde, R. Surface Modification of Oxidic Nanoparticles Using 3-Methacryloxypropyltrimethoxysilane. *J. Colloid Interface Sci.* **2004**, *269*, 109−116.
(52) Rong, Y.; Chen, H.-Z.; Li, H.-Y.; Wang, M. Encapsulation of Titanium Dioxide Particles by Polystyrene via Radical Polymerization. *Colloids Surf., A* **2005**, *253*, 193−197.
(53) Rong, Y.; Chen, H.-Z.; Wu, G.; Wang, M. Preparation and Characterization of Titanium Dioxide Nanoparticle/Polystyrene Composites via Radical Polymerization. *Mater. Chem. Phys.* **2005**, *91*, 370−374.
(54) Nyquist, R. A. *Interpreting Infrared, Raman, and Nuclear Magnetic Resonance Spectra*; Academic Press: San Diego, 2001.
(55) Trasferetti, B. C.; Davanzo, C. U.; Bica de Moraes, M. A. LO-TO Splittings in Plasma-Deposited Siloxane Films. *J. Phys. Chem. B* **2003**, *107*, 10699−10708.
(56) Bexell, U.; Olsson, M. Characterization of a Non-Organofunctional Silane Film Deposited on Al, Zn and Al−43.4 Zn−1.6 Si Alloy-Coated Steel. *Surf. Interface Anal.* **2001**, *31*, 223−231.
(57) Zou, H.; Wu, S.; Shen, J. Polymer/Silica Nanocomposites: Preparation, Characterization, Properties, and Applications. *Chem. Rev.* **2008**, *108*, 3893−3957.
(58) Benoit, R.; Durand, Y.; Narjoux, B.; Quintana, G. Lasurface; http://www.lasurface.com/ (accessed May 28, 2014).
(59) Fellows, C. M. In *Polymer Grafting and Crosslinking*; Bhattacharya, A., Rawlins, J. W., Ray, P., Eds.; John Wiley & Sons: New York, NY, USA, 2008; Chapter 3: Mechanism and Kinetics, pp 66−70.
(60) Grundmeier, G.; Schmidt, W.; Stratmann, M. Corrosion Protection by Organic Coatings: Electrochemical Mechanism and Novel Methods of Investigation. *Electrochim. Acta* **2000**, *45*, 2515−2533.
(61) Yasuda, H.; Yu, Q.; Chen, M. Interfacial Factors in Corrosion Protection: An EIS Study of Model Systems. *Prog. Org. Coat.* **2001**, *41*, 273−279.
(62) Plueddemann, E. P.; Pape, P. G.; Bank, H. M. New Coupling Agents for Improved Corrosion-Resistant Composites. *Polym.-Plast. Technol. Eng.* **1986**, *25*, 223−231.
(63) Watts, J. F.; Rattana, A.; Abel, M.-L. Interfacial Chemistry of Adhesives on Hydrated Aluminium and Hydrated Aluminium Treated with an Organosilane. *Surf. Interface Anal.* **2004**, *36*, 1449−1468.
(64) Abel, M.-L.; Watts, J. F. Examination of the Interface of a Model Adhesive Joint by Surface Analysis: A Study by XPS and ToF-SIMS. *Surf. Interface Anal.* **2009**, *41*, 508−516.
(65) Pourbaix, M. *Atlas of Electrochemical Equilibria in Aqueous Solutions*; National Association of Corrosion Engineers/Centre Belge d'Etude de la Corrosion CEBELCOR: Houston/Bruxelles, 1974.
(66) Nayak, S.; Biedermann, P. U.; Stratmann, M.; Erbe, A. A Mechanistic Study of the Electrochemical Oxygen Reduction on the Model Semiconductor n-Ge(100) by ATR-IR and DFT. *Phys. Chem. Chem. Phys.* **2013**, *15*, 5771−5781.
(67) Nayak, S.; Biedermann, P. U.; Stratmann, M.; Erbe, A. In Situ Infrared Spectroscopic Investigation of Intermediates in the Electrochemical Oxygen Reduction on n-Ge (100) in Alkaline Perchlorate and Chloride Electrolyte. *Electrochim. Acta* **2013**, *106*, 472−482.
(68) Sørensen, P.; Weinell, C.; Dam-Johansen, K.; Kiil, S. Reduction of Cathodic Delamination Rates of Anticorrosive Coatings Using Free Radical Scavengers. *J. Coat. Technol. Res.* **2010**, *7*, 773−786.
(69) Posner, R.; Marazita, M.; Amthor, S.; Roschmann, K.; Grundmeier, G. Influence of Interface Chemistry and Network Density on Interfacial Ion Transport Kinetics for Styrene/Acrylate Copolymer Coated Zinc and Iron Substrates. *Corros. Sci.* **2010**, *52*, 754−760.